# Precipitation of Phosphorus, Arsenic, and Boron in Thin Silicon Foils

Abstract: Diffusion of high concentrations of P, B, and As in thin foils of silicon of (111), (110), and (100) orientations is shown to result in extensive precipitation. Observation of the precipitates through a transmission electron microscope has indicated that phosphorus diffusion gives rise to precipitate platelets. Boron precipitates were found to be of various shapes—rod, platelet, and three-dimensional. Matrix contrast observation showed that small coherent platelets of P and B are both of the "vacancy" type—this is in accordance with the smaller size of B and P atoms in the silicon matrix. Contrast studies for arsenic precipitates were inconclusive. Helical dislocations oriented along  $\langle 220 \rangle$  directions and originating from precipitate regions were observed in the phosphorus-diffused foils; boron precipitates showed no such helices. Boron rods and three-dimensional structures, however, were invariably found to be enveloped by dislocation spirals, with Burgers vector different from the usual  $a/2 \langle 110 \rangle$  type. These dislocation envelopes are thought to be interfacial dislocations. It is concluded that the precipitates are not identifiable as discrete SiP or Si<sub>x</sub>B<sub>y</sub> phases, since these phases would be expected to cause compression in the matrix because their specific volume is higher than that of silicon.

#### Introduction

Precipitation of impurities belonging to the III and V columns in the Periodic Table is known to occur in silicon when the impurity concentrations reach the limit of solid solubility. The precipitates of phosphorus in the form of rods have been observed by Thomas¹ in a heavily doped silicon after a suitable aging treatment. Silicon wafers diffused with phosphorus have also been known² to contain such precipitates when the surface concentration of the diffusant is higher than  $10^{20}$  atoms/cm³. These observations were, however, limited to the precipitation effects in bulk silicon. Besides, particularly little is known about the precipitation of As and B in silicon.

In this article, we present the results of a detailed study, using transmission electron microscopy, of the precipitate structures found after diffusion of high amounts of P, B, and As in thin foils of silicon. It has been reported<sup>3</sup> that precipitation is more extensive in thin foils of silicon than in bulk silicon wafers. The thin-foil precipitation method involves diffusion in small samples already thinned (to about 4000 to 8000Å thickness) and ready for examination through the microscope.

Morphologies of the precipitates induced by diffusion of P, B and As in thin silicon foils are presented in this article. Formation of massive precipitate platelets of phosphorus on {111} planes and oriented along (220) directions in the thin-foil silicon matrix has been reported earlier. These platelets, when thick, are also known to cause slip and stacking faults in the silicon matrix, indicating that precipitation stresses rise faster than they can be relieved

by "thermal relaxation" or "recovery," a process in which lattice adjustment occurs by a disorganized diffusive movement of the atoms. The nature of the coherency strains in the matrix associated with the small precipitate structures is discussed. Precipitation mechanisms are also indicated.

## **Experimental**

For diffusion, small circular samples (3 mm in diameter) were obtained from high resistivity ( $10\Omega$ -cm) 5-mil-thick silicon wafers of  $\langle 111 \rangle$ ,  $\langle 110 \rangle$ , and  $\langle 100 \rangle$  orientations. The silicon wafers were cut from Czochralski-grown crystals of the various orientations and were treated chemically for removal of surface damage after lapping. Small circular samples, obtained from these wafers and thinned (Fig. 1) chemically to within a few thousand angstroms by the usual means provided enough area for transmission microscopy.

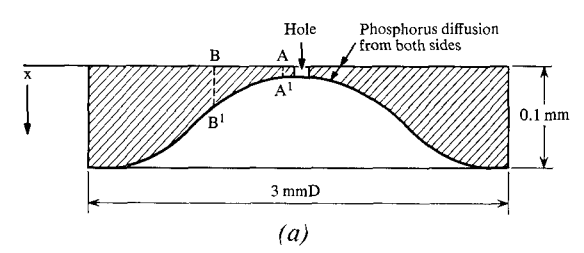
Samples after thinning were subjected to diffusion from the sources  $P_2O_5$ , As and B. The diffusion of phosphorus was carried out in an open-tube configuration at  $970^{\circ}$  C. As and B were diffused in capsules, the details of which may be found elsewhere. The diffusion data for the various diffusion sources and the crystal orientations are presented in Table 1. The data in this table are based upon electrical measurements on the test-wafers used for diffusion along with the small circular samples. The surface concentrations are based on measurements of surface resistivity and the ideal erfc distribution of the diffusant.

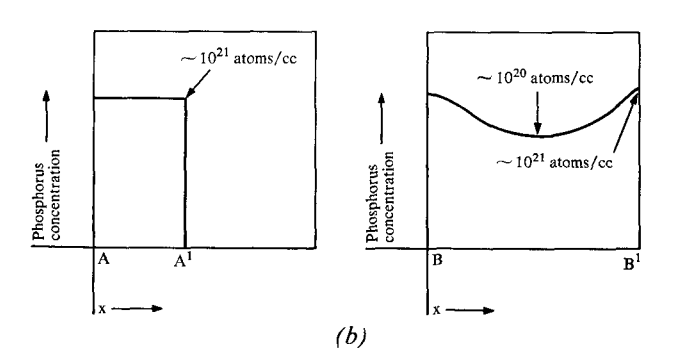
Table 1. Diffusion data based on test wafers.

Silicon orientations	Diffusion temperature, °C	Source	Surface concentration, atoms/cm³	Junction depth, microns	Diffusion system
⟨111⟩	1000	$P_2O_5$	$1.4 \times 10^{21}$	10	Open-tube furnace
⟨111⟩ ⟨110⟩ ⟨100⟩	970	$P_2O_5$	$9 \times 10^{20}$	10	Open-tube furnace
(111 ) (110 ) (100 )	1200	As	$7 imes10^{20}$	10	Closed quartz capsule technique
⟨111⟩ ⟨110⟩ ⟨100⟩	1000	В	$2.6\times10^{20}$	7	Closed quartz capsule technique

The expected phosphorus distributions in the thinned circular samples are shown in Fig. 1. (The other impurities should show similar distributions.) The important point to be noted here is that there should exist almost no concentration gradient in the AA' region, because the thickness of the foil involved is far less ( $\approx 0.5\mu$ ) than the expected junction depth which is  $\approx 10\mu$ . A gradient of impurity exists in thicker regions such as BB'. This would also imply that there could exist a flow of matter in the planes parallel to the sample surface.

Figure 1 Phosphorus distribution in AA' and BB' regions of a small sample chemically thinned from one side for observation with a transmission electron microscope (diffusion source  $P_2O_5$ ).





#### • Phase equilibrium

A systematic study of precipitation of the impurities usually diffused in silicon for making transistor structures is seriously limited for the present due to inadequate knowledge of the equilibrium phase diagrams. The Si-B system is not yet known. In Figs. 2a and 2b, Si-P and Si-As systems<sup>6,7</sup> are presented. These diagrams lack information particularly in the regions of terminal solid solutions, wherein lies our interest. Moreover, the existence of the different phases in these diagrams has never been conclusively established.

The information in the region of terminal solid solutions in Figs. 2a and 2b has been developed by using the data compiled by Trumbore. There exists a wide discrepancy, however, in the values of solid solubility limits; therefore the accuracy of the solvus curves in these figures cannot be relied upon. The data obtained by Trumbore on the solid-solubility limits are presented in Fig. 3.

It cannot be said with certainty whether the precipitation occurs during cooling from the diffusion temperature or during the diffusion process itself at the high temperature. The thin foil sample is expected to cool down very rapidly on removal from the diffusion furnace and, consequently, the reduction in the impurity solubility with decreasing temperature should give rise to the nonequilibrium precipitate structures, coherent with the matrix.

The possibility of precipitation during the diffusion process itself also exists if the solubility of the impurity diminishes because of the introduction of strain by the impurity. A high state of strain is in fact created during diffusion of a large amount of P, the atoms of which have a considerable atomic misfit in silicon. This is evidenced by the generation of misfit dislocation grids in silicon diffused with high amounts of phosphorus. The diffusivity of phosphorus in Si is known<sup>10</sup> to rise almost asymptotically with its concentration in the range  $10^{20}$  to  $10^{21}$ 

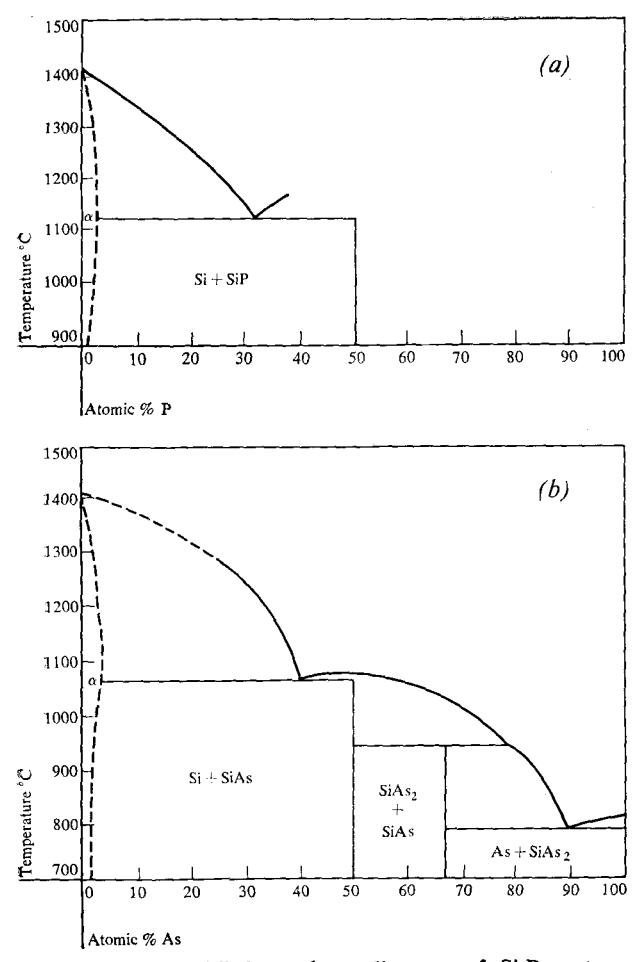


Figure 2 (a) Equilibrium phase diagram of Si-P system; (b) equilibrium phase diagram of Si-As system.

atoms/cm<sup>3</sup>. One possible implication of this observation is the diminishing solid solubility of phosphorus with the increase in strain. We feel, however, that in the absence of firm evidence for this kind of precipitation, the occurrence of precipitation during cooling down from the diffusion temperature is most likely.

# Electron microscopic observations

# • Phosphorus precipitation

# Morphology

The precipitates were found to be platelets lying on the planes  $\{111\}_{si}$  in all the three orientations of silicon wafers, viz., (111), (110), and (100). The traces of the platelets were found invariably to be the intersection of  $\{111\}_{si}$  planes with the foil planes. Figures 4a, 4b, and 4c are representative observations of the platelets formed in wafers of

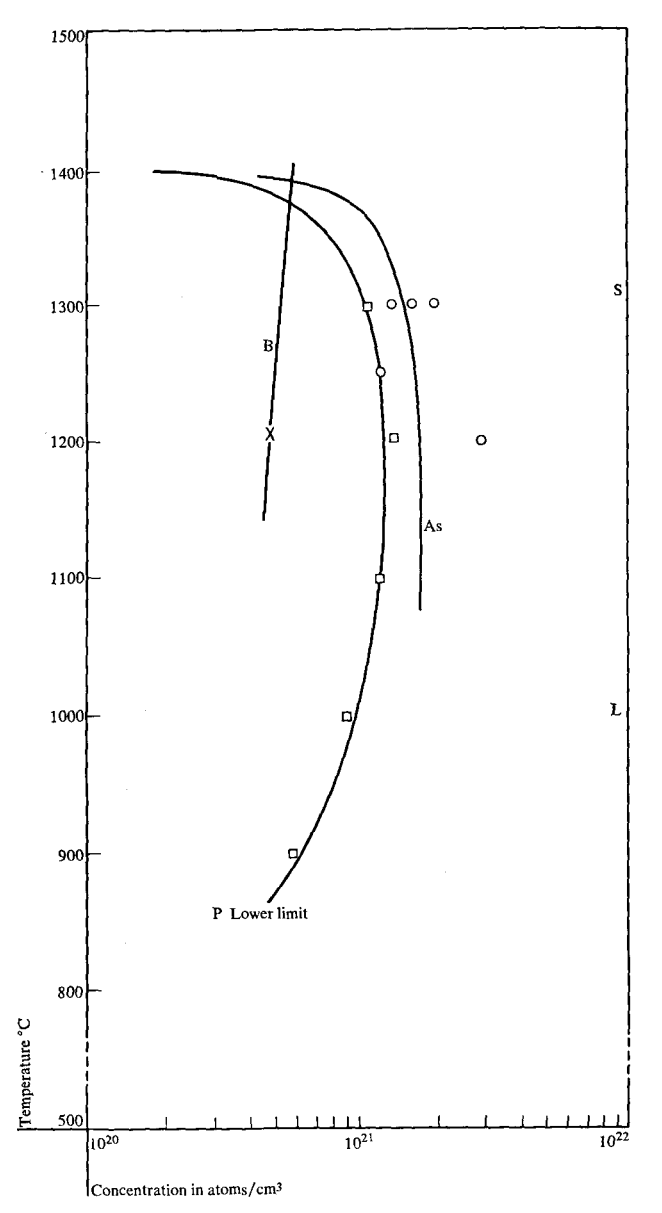


Figure 3 Solid solubilities of P, B and As in silicon.

different orientations. In Fig. 4e displacement fringe<sup>11</sup> contrast is observed in a highly magnified bundle of platelets formed in a (111) foil. The most characteristic property of displacement fringes is that they define regions of constant depth in the foil and hence, on a planar precipitate, they run parallel to the line of intersection of the precipitate platelet and the foil surfaces. Figure 4f shows a selected area diffraction pattern corresponding to the relatively thin platelet structure (Fig. 4c) observed on a (100) foil. In this figure, one observes streaking along  $\langle 220 \rangle$  directions which are perpendicular to the traces of the platelets lying on  $\{111\}_{si}$  planes. In the dense precipitate regions

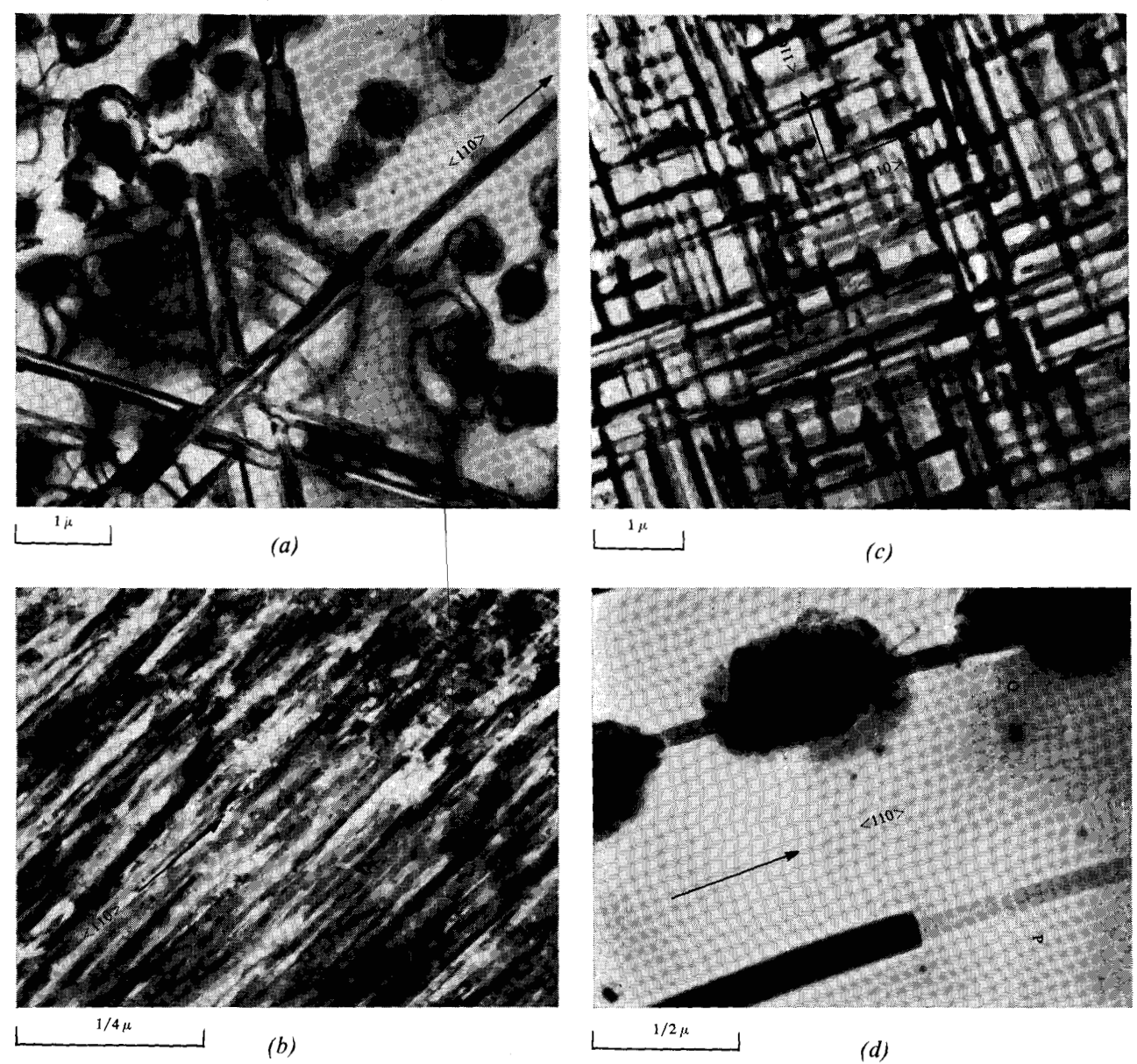


Figure 4 Long precipitates of phosphorus for concentrations  $> 10^{21}$  atoms/cm³. (a) Platelets in (111) film. Note also the regions of circular dark contrasts which are due to phosphorus rich clusters. (b) Thin precipitates oriented along (110) direction in (110) film. (c) Thin precipitate platelets oriented along (110) direction in (100) film. (d) Stacking faults originating from thick precipitate platelets. Note also the decoration of the fault Q by phosphorus clusters.

diffraction patterns giving rise to both streaking and the phenomenon of double diffraction<sup>11</sup> were also observed, as illustrated in Fig. 4g.

The (111) and (100) silicon foils show platelets lying on three sets of  $\{111\}_{\rm Si}$  and four sets of  $\{111\}_{\rm Si}$  respectively. However, in the case of (110) foil, the precipitate platelets were observed on those  $\{111\}_{\rm Si}$  planes (Fig. 4b) which were not perpendicular to the surface of the foil.

The lengths of precipitate platelets obtained at concentrations of phosphorus greater than 10<sup>21</sup> atoms/cm<sup>3</sup> are much larger than the lengths of those obtained at lower

concentrations (see Figs. 4 and 6). The long precipitate platelets on higher magnification invariably revealed displacement fringes. On the other hand, the small precipitate platelets exhibit strong coherency strain contrasts, as illustrated in Fig. 6a. Coherency contrasts associated with the long precipitate platelets were often found undistinguishable from the absorption contrasts because of the high density of the platelets.

Some precipitate platelets (Fig. 4d) were occasionally observed to give rise to stacking faults at their tips.<sup>3</sup> This is possible when a platelet becomes thick enough to cause

274

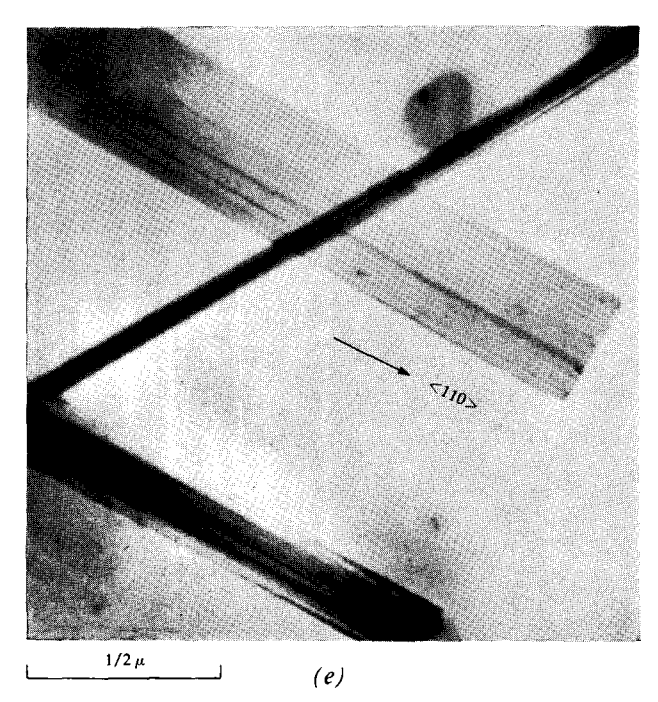


Figure 4 (e) Displacement fringes in the platelets observed in (111) silicon film. (f) Selected area diffraction pattern obtained from a region in Fig. 4c where relatively thin platelets are observed. Note the broadening of the reciprocal points along (220) directions. The strong reflections observed are of (004) type. (g) Selected area diffraction pattern in the region of dense structures of precipitates in (100) film. Note the intense double diffraction phenomenon.

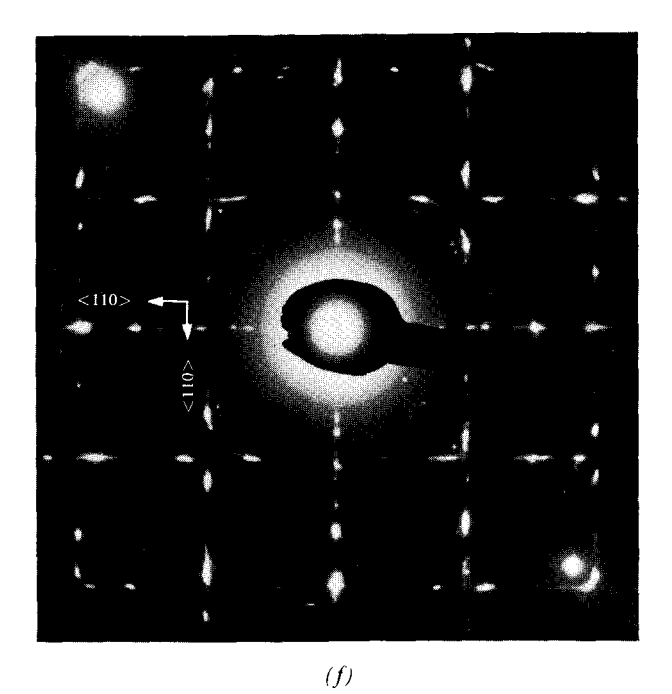
deformation of the thin foil because of volume changes and differential thermal contraction accompanying the precipitate formation.

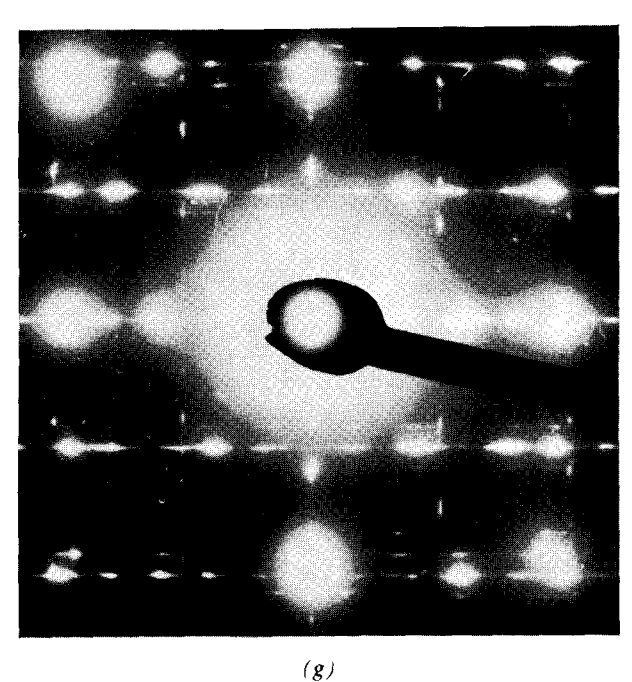
Regions of uniform circular contrast are also observed in Fig. 4a. These are interpreted to be due to clusters of phosphorus. Such structures were occasionally observed (Fig. 4d) to decorate stacking faults. This is an example of heterogeneous nucleation of precipitates, wherein strain energy is released by the transfer of solute to the stacking faults.

It has been shown<sup>3</sup> that the area density of the precipitates in {111} foils decreases as thickness increases. Instead, misfit dislocations are observed in thick foil regions. This is understandable since steep impurity gradients (and therefore, strain gradients) exist in the thick foil regions (see Fig. 1). In the thinner foil regions precipitation is favored.

## Lattice mismatch

It is well known that when two thin crystals of the same or similar crystal structure are superposed with a small orientation difference or with slightly different spacings, Moiré fringes result. Moiré fringes were observed for precipitate plates occasionally lying on the foil surface.





This is illustrated in Fig. 5. The fringe spacing varied from 200 Å to 500 Å for  $\langle 220 \rangle$  prominent reflections. The fringe spacing M is given by the formula

$$M = \frac{d_{\rm Si}d_{ppt}}{d_{\rm Si} - d_{ppt}} \approx d_{\rm Si}^2/\Delta d, \qquad (1)$$

where d represents interplanar spacing for a particular reflection. Substituting  $d_{(220)} = 1.920$  Å for silicon,  $\Delta d/d_{\rm Si}$  is found to range from 0.96% to 0.38%.

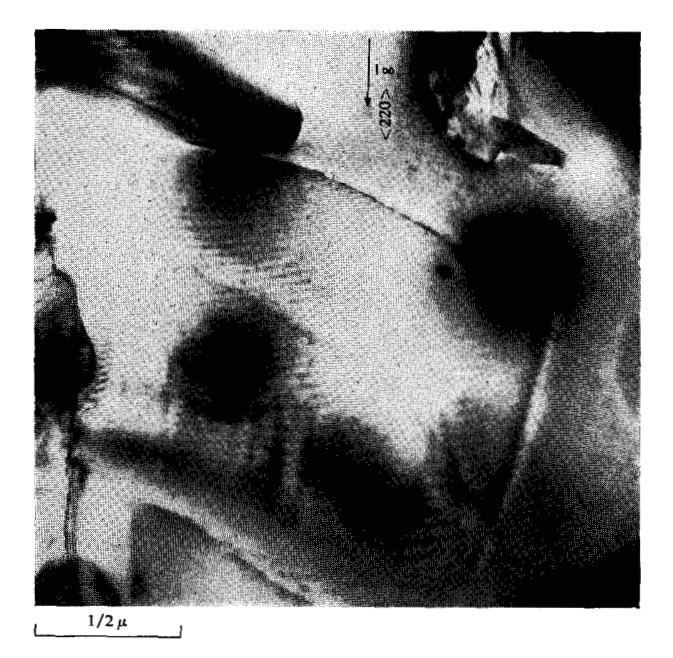
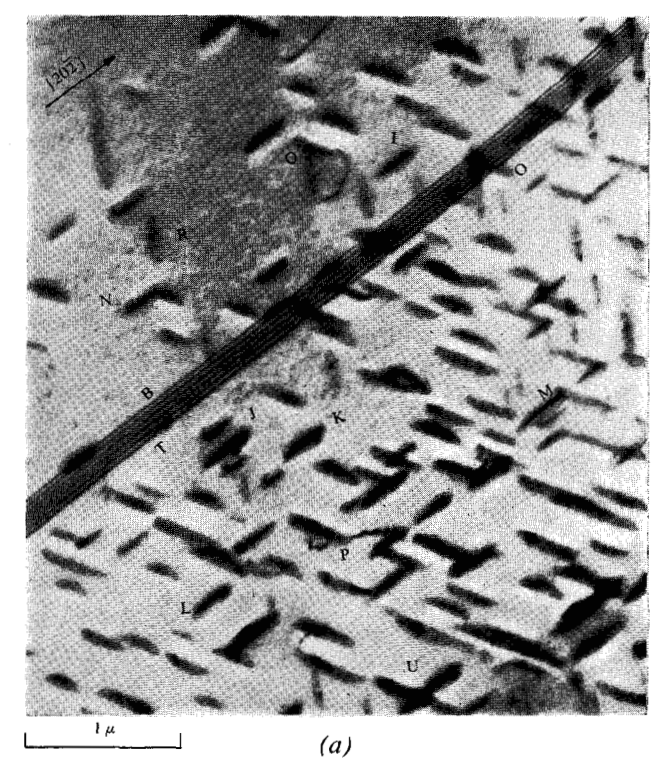


Figure 5 Moiré fringes in the precipitate platelets lying parallel to the film surface. This is a bright field view with a strongly operating (220) reflection.



#### Matrix contrast

The small precipitate platelets (Fig. 6a) in the case of phosphorus concentrations less than 10<sup>21</sup> atoms/cm<sup>3</sup> show a considerable amount of strain contrast in their vicinity. Figures 6b and 6c show the two dark-field views which illustrate this point. These two dark-field views with the different operating reflections correspond to the tilts of the bright-field view of Fig. 6a. With a single strong operating diffracting plane (two-beam case), the white contrast is always found on the same side of the positive g (the diffraction vector) direction in a printed micrograph. The correct sense of g was obtained by taking into account both the electron-optical rotation and the relative inversion of the micrographs and the diffraction pattern.<sup>12</sup> The precipitates, therefore, are of vacancy type, indicating thereby that the silicon matrix surrounding the platelets is under tension. This interpretation is based on the work of Ashby and Brown.13

In Fig. 6c, one also observes the vanishing of the large stacking fault running along the  $[20\overline{2}]$  (g also equal to  $[20\overline{2}]$ ) direction through the bright-field in Fig. 6a. This indicates that the fault obeys the phase-contrast rule<sup>14</sup> applicable to faults formed by shear of type  $1/6 \langle 121 \rangle$  on a (111) type plane. The stacking fault is also identified as an intrinsic fault. From the expected pseudo-complementary contrast for the bottom side of B of the fault in the dark field (Fig. 6b), the sense of the slope of the fault plane was determined. The intrinsic nature of the fault is indicated

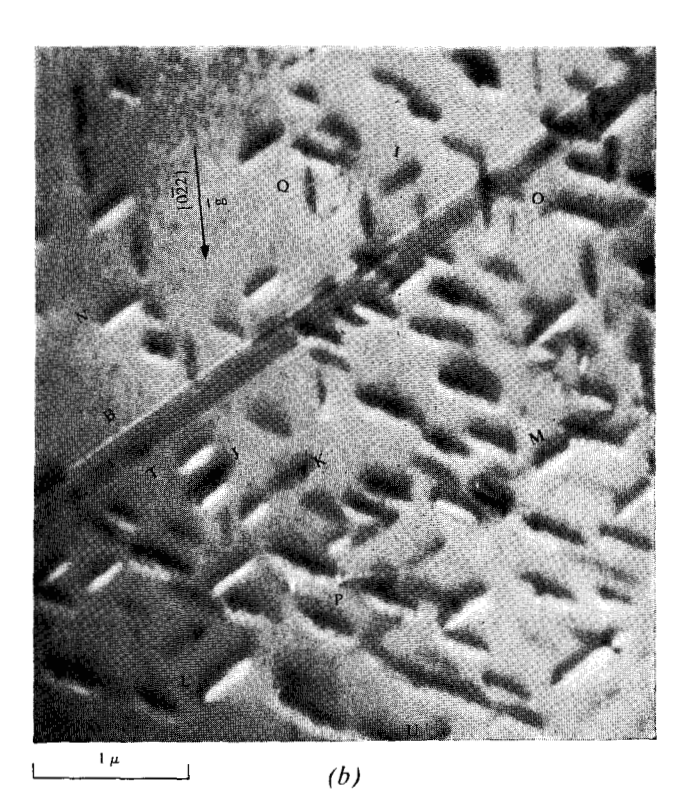
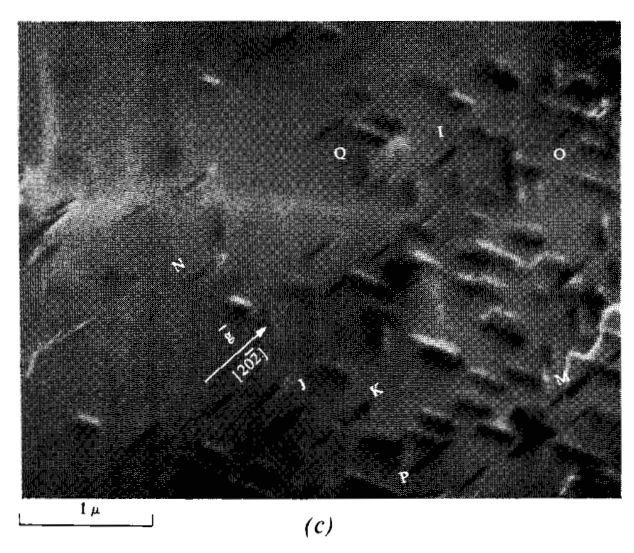


Figure 6 Small precipitates of phosphorus for concentrations  $> 10^{21}$  atoms/cm<sup>3</sup>. (a) Bright-field view of platelet type precipitates; (b) dark-field view of Fig. 6a with  $[0\bar{2}2]$  as the operating reflection.

276



**Figure 6** (c) Dark-field view of Fig. 6a with  $[20\overline{2}]$  as the operating reflection.

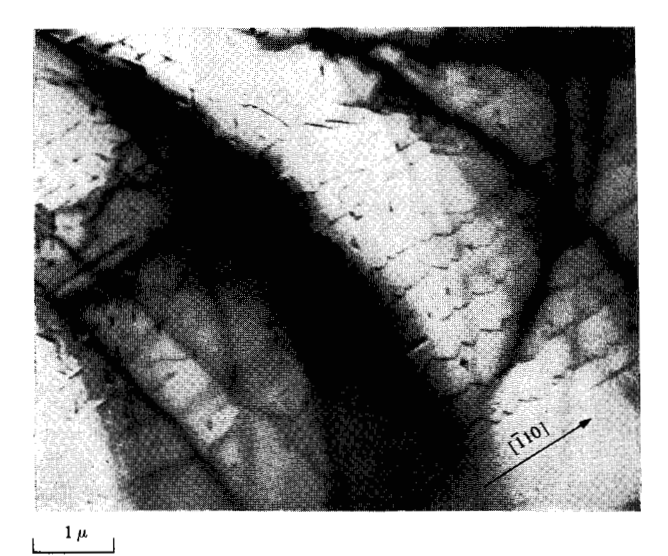


Figure 7 Helical dislocations emanating from precipitate structures.

by the facts<sup>12</sup> that the positive g is to the right of the fault that slopes upwards towards the right and that the first fringe is dark in the bright-field view of Fig. 6a.

# Helical dislocations

Frequently, in the thicker regions of the foils, helical dislocations rising from precipitate regions were observed; this is seen in Fig. 7. The density of these dislocations was measured in some regions to be as high as 10<sup>9</sup> lines/cm<sup>2</sup>. The minimum radius of the helices was found to be about 500 Å and the pitch was of the same order. The maximum radius and the maximum pitch were 1150 Å and 2300 Å respectively. The well-developed helices oriented themselves along (110) directions invariably. The appearance of helical dislocations originating at the precipitation sites, e.g., P and Q in Fig. 6a (and also in Fig. 7) has some significance with regard to the possible precipitation mechanism. (This is discussed later.) The existence of the helices implies either supersaturation or undersaturation of vacancies.

#### • Arsenic precipitation

Figures 8a and 8b show the precipitation of arsenic in silicon wafers with (111) and (100) orientations respectively. In contrast with phosphorus precipitation which is distinctly massive, we observe precipitates of arsenic to be minute clusters with diffuse spotty contrasts. Occasionally, large clusters of arsenic are observed to emit dislocations. The traces of {111}<sub>si</sub> planes are seen to be delineated with small clusters of arsenic in Fig. 8a. These traces are most likely to be slip steps introduced during diffusion. A square array of precipitate structures on the

(100) foil is observed in Fig. 8b. Selected area diffraction study did not show perceptible streaking.

### • Boron precipitation

## Morphology

One, two and three-dimensional precipitate structures were observed in silicon foils of all orientations after diffusion of large amounts of boron. All these structures are observed in Fig. 9, which is a bright-field micrograph for a (110) foil. Precipitate structures A precisely oriented along  $\langle 220 \rangle$  directions were found by tilting experiments to be platelets (two-dimensional). In Fig. 9, one also observes structures B approximately oriented along  $\langle 224 \rangle$  directions and identified as rods (one-dimensional). Structures C oriented again approximately along  $\langle 224 \rangle$  directions were observed to be three-dimensional. We examine next both the matrix contrast and the precipitate contrast in detail by observing these structures at higher magnifications.

#### Matrix contrast

Figure 10 shows the platelet-type boron precipitates in a (100) foil. This is a dark field micrograph with  $g = [\overline{2}20]$ . The bright matrix contrast in the print was consistently observed in the direction of positive g with the vector representing deviation from the reciprocal lattice point, i.e.,  $s \approx 0$ . This indicated that these precipitates are also of the vacancy type, which is in accordance with the consideration that boron atoms are smaller in radius than silicon atoms. Selected area diffraction in the precipitate regions showed streaking along  $\langle 220 \rangle$  directions similar to that in the case

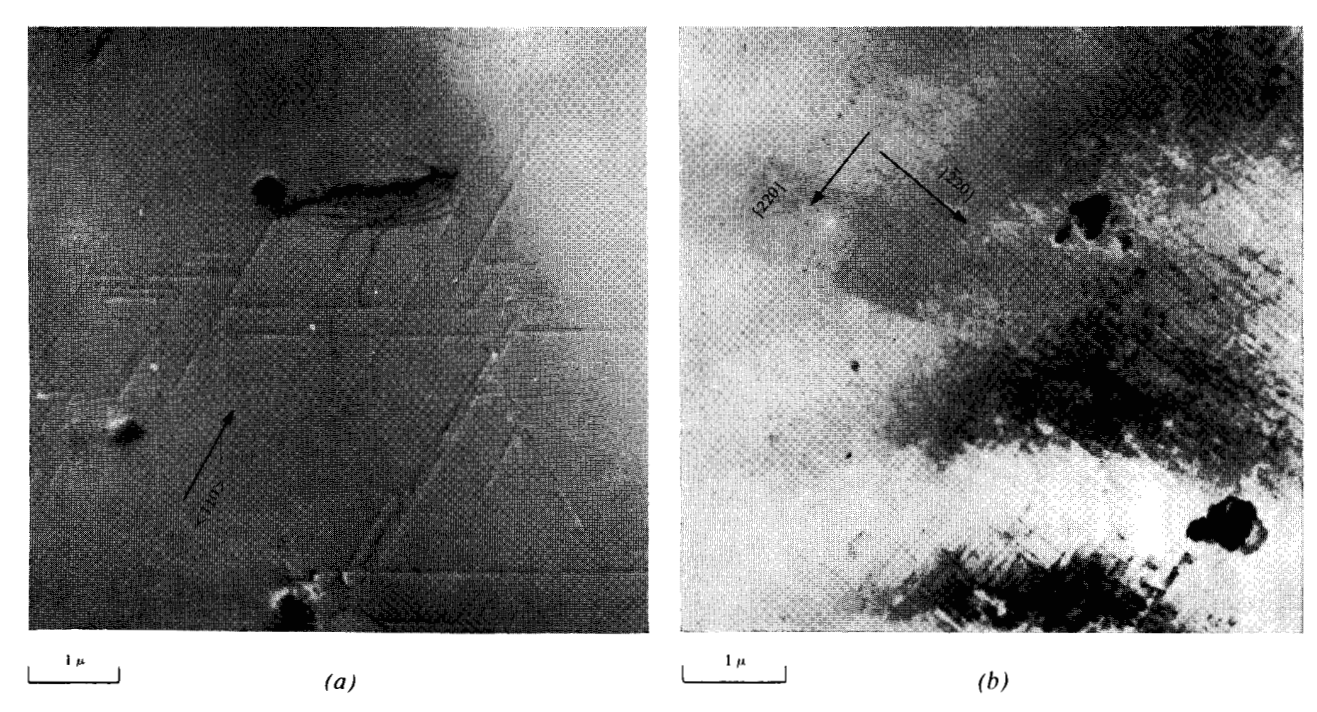


Figure 8 Arsenic precipitates: (a) decoration of slip traces in (111) film by arsenic clusters; (b) square array of arsenic precipitates in (100) film.

Figure 9 Boron precipitates in (110) film. Precipitates designated by letter A are platelets, by letter B, rods and by letter C, three-dimensional structures.

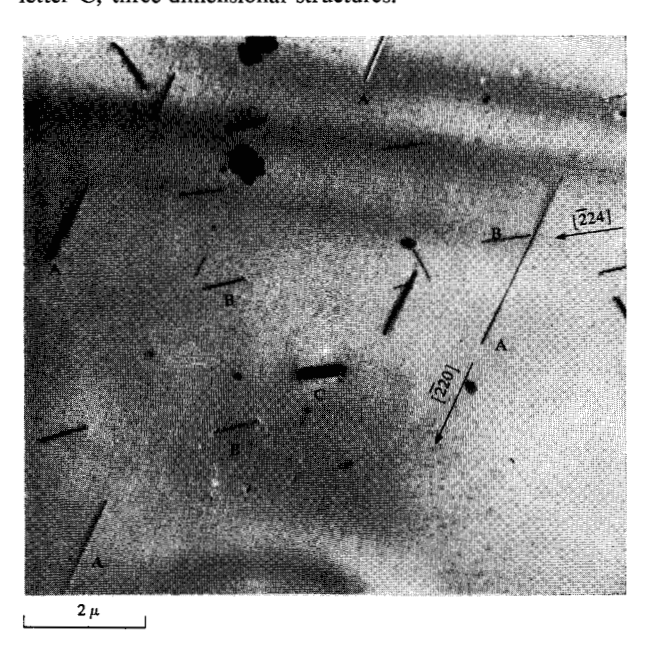
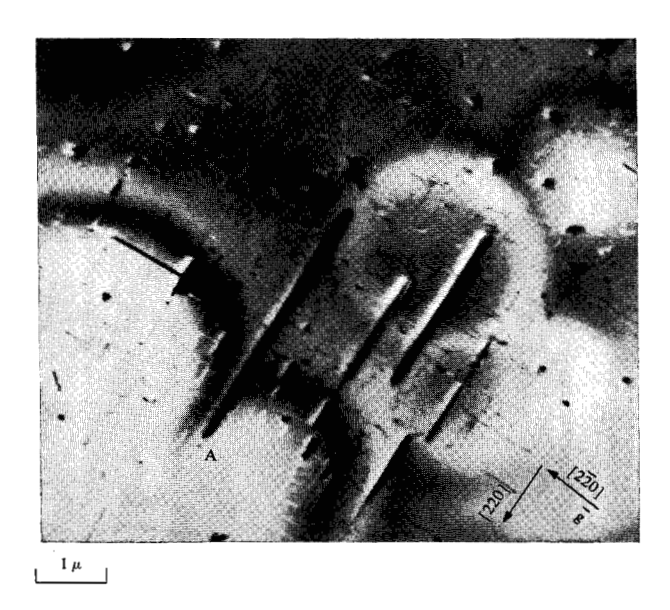


Figure 10 Platelet type boron precipitates in (100) foil. This is a dark field view with operating reflection  $g = [2\overline{2}0]$ .



of P precipitation. Consequently, the platelets do lie on  $\{111\}_{\rm Si}$  planes. Very fine linear structures extending in  $\langle 220 \rangle$  directions can also be observed in Fig. 10. It was not possible to identify them, but they are interpreted to be stringlets of precipitate.

Figures 11a-11d show the details of the rod-shaped precipitates B and the platelets A observed in Fig. 9. The micrograph in Fig. 11b is a dark-field view corresponding to the bright-field view in Fig. 11a and the operating reflection  $[1\overline{1}1]$ . Single or double helices enveloping the rod

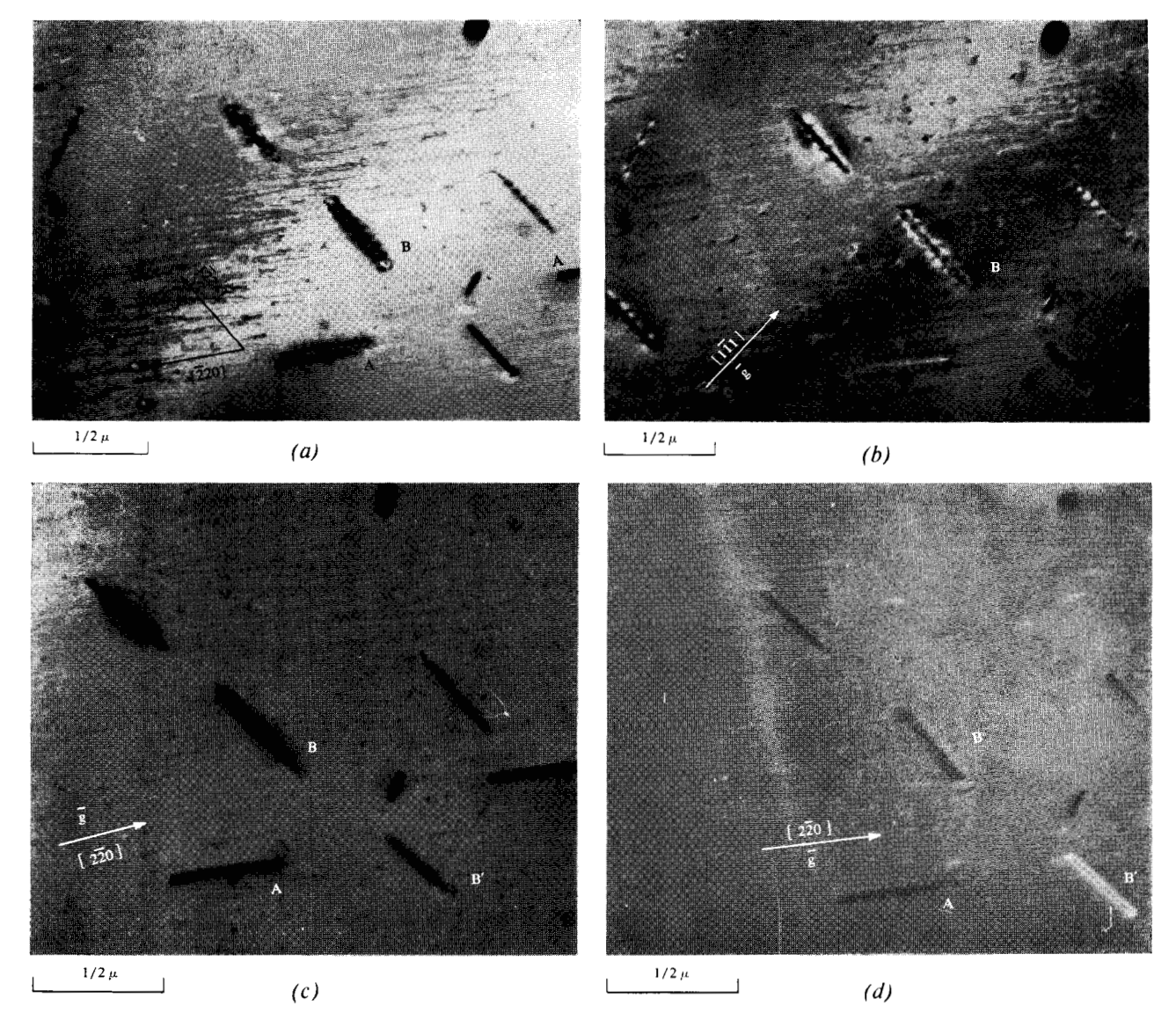


Figure 11 Precipitates of boron in (110) film: (a) magnified bright field view corresponding to a region in Fig. 9; (b) dark field view of Fig. 11(a) with  $\mathbf{g} = [1\overline{1}1]$ ; (c) bright field view corresponding to Fig. 11(a) with the strong operating reflection [2\overline{20}]; (d) dark field view of Fig. 11(c) with  $\mathbf{g} = [2\overline{20}]$ . (Note the absence of asymmetrical matrix contrast in the vicinity of the rods entwined by interfacial dislocations.)

type precipitates are invariably observed. On tilting the foil, the helix patterns can be made to disappear as shown in Fig. 11c, which is a bright-field view with a strong  $[2\bar{2}0]$  reflection. The helix patterns are therefore taken to be dislocations. Figure 11d is the dark-field view corresponding to Fig. 11c with  $g = [2\bar{2}0]$ . The matrix contrast is unobservable near the rods and the particular structure B' is a good example of this. No unambiguous determination of the Burgers vector of the helix envelopes was possible. However, vanishing of the dislocation contrast for the  $[\bar{2}20]$  reflection using the criterion  $(g \cdot b) =$ 

0 signifies that the vector of the type  $(a/2) \langle 110 \rangle$ , i.e.,  $(a/2) [\overline{1}10]$ , is not the b. Also the vector (a/2) [110] cannot be the b, since for the reflection  $[1\overline{1}1]$ , the contrast of the helix is strong. Therefore, the Burgers vector of the helix envelope cannot be of  $(a/2) \langle 110 \rangle$  type. For this reason, a different b has to be assumed (possibly a [001]), and this implies that the helical envelopes are probably the mismatch boundary dislocations around the precipitate rods.

The three-dimensional boron precipitates also show (Figs. 12a, 12b) mismatch boundary dislocations. Figure

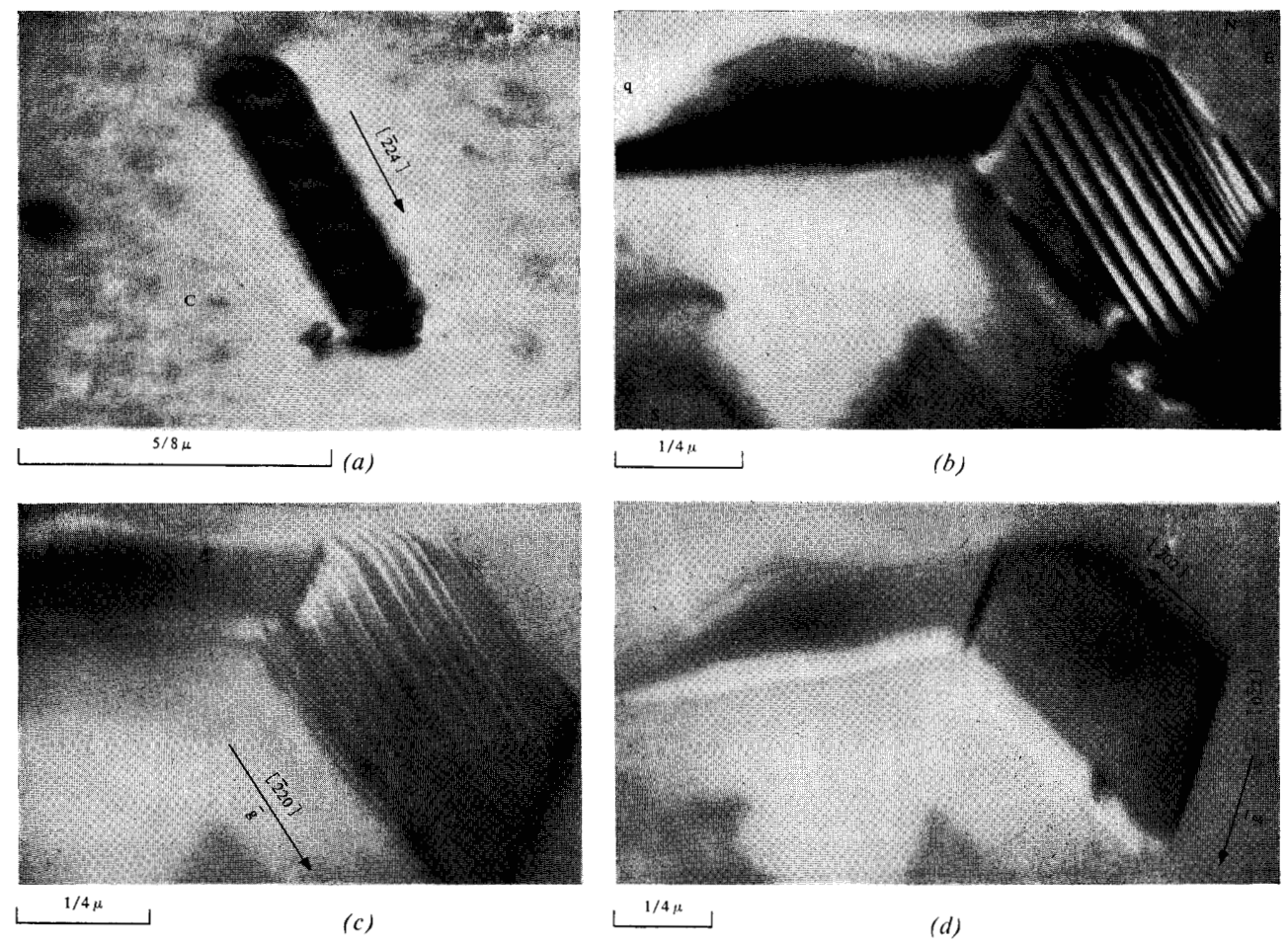


Figure 12 Three-dimensional precipitates of boron. (a) Magnified view of structure C observed in Fig. 9. Note the interfacial dislocations. (b) A large three-dimensional boron precipitate enveloped by a dislocation helix. The pitch of the helix is increasing from E-N direction to S-W direction. (c) Dark field view of Fig. 11(b) with  $g = [\bar{2}20]$ . (d) Dark field view of Fig. 11(b) with  $g = [0\bar{2}2]$ .

12a is the magnified image of the structure C observed in Fig. 9. The envelope character of the mismatch boundary dislocation is apparent in Fig. 12b, which is a bright-field view in an area of a (111)-oriented foil. The pitch of the dislocation envelope is observed to increase from East-North direction towards South-West in this figure. Figure 12c is a dark-field with  $g = [\overline{2}20]$  showing excellent complementary contrast. With  $g = [0\overline{2}2]$ , the dislocation envelope is observed to vanish (Fig. 12d) in the same fashion as the helical envelopes for the boron rods.

## Discussion

A brief summary of the results of the electron microscopic study of precipitation of P, B, and As in silicon is presented in Table 2. The following discussion is aimed at explaining the major features therein. Because of the insufficient data on arsenic precipitation, only precipitation of phosphorus and boron will be discussed in detail.

As seen in Fig. 2c, both phosphorus and boron show decreasing solubilities at lower temperatures. Therefore, on cooling, the thin foil will show supersaturation of the solutes provided the foil is saturated at the diffusion temperature.

Precipitates of platelet type observed in the case of both phosphorus- and boron-diffused thin foils are of vacancy type. The precipitating phase consequently is of smaller specific volume than that of silicon. This will be true if the precipitates observed are rich in phosphorus or boron atoms, which are smaller than silicon atoms.<sup>4</sup> The precipitates observed, however, cannot be named as SiP or Si<sub>x</sub> B<sub>y</sub> phases. Compounds of silicon with impurities such as P, B, and As are described in the literature as having larger specific volumes (with exception of Si B<sub>3</sub>) than that of Si.<sup>16</sup> Thomas also observed vacancy type precipitates of rod geometry in silicon heavily doped with phosphorus after a suitable aging treatment, and he called them phosphorus rods.<sup>1</sup> There seems to be no indication

Table 2. Precipitation data.

	Phosphorus	Boron	Arsenic
Atom size (silicon atom radius = 1.17 Å)	1.10 Å	0.88 Å	1.18 Å
Precipitate morphology	Platelets lying on {111} silicon plane	Rods (one dimensional), platelets (two dimensional), and three dimensional struc- tures	Clusters of arsenic decorate {111} silicon planes.
Matrix strain	Tension in the matrix sur- rounding platelets	Tension in the matrix surrounding platelets	Could not be established.
Precipitate type (platelets)	Vacancy	Vacancy	Could not be established.
Dislocations	Helices due to nonequilibrium vacancies	Helical envelopes as mismatch boundary	Dislocations due to concentration fluctuations.
Stacking faults	Emission of split dislocations by thick platelets at their tips		
Moiré fringes  Observed in platelets parallel to the foil surface. Fringe spacing for ⟨220⟩ reflection  ≈ 220/500 Å		Rare observation	Not found.
Diffraction pattern	Streaking	Streaking	

that points towards formation of a definite SiP phase.

According to the crystal shape theorem, thin precipitates produce the diffraction effects of a two-dimensional lattice, i.e., the reciprocal lattice points are extended in a direction parallel to the smallest dimensions of the crystal. The observations of seemingly continuous streaks in (220) directions for (100) foil containing thin precipitate platelets oriented along (220) directions is in accordance with the shape theorem, if we assume that we have extension of rel rods perpendicular to {111} planes which intersect the foil along (220) directions. The elongation of reciprocal lattice points was observed for all orientations of the thin films and in the case of both P and B precipitate structures. Consequently, it is felt that we may have pre-precipitation stages like Guinier-Preston zones. Some of the zone structures are expected to grow into the discrete precipitate structures that are observed.

# Phosphorus precipitation

The occurrence of long dislocation helices oriented along  $\langle 220 \rangle$  directions in the phosphorus precipitate regions of Fig. 7 and short helices in Fig. 6a are indicative of the existence of non-equilibrium vacancy concentrations. The mechanism of formation of such helices is well-known.<sup>17</sup> The non-equilibrium vacancy concentrations may be attributed to four different mechanisms: (1) quenching of the foils, (2) dissociation of vacancies bound with

solute atoms due to decrease in solubility of the solute with temperature, (3) the attraction of vacancies toward compressed regions and (4) possible conversion of substitutional atoms into interstitials and vacancies during precipitation. The last three mechanisms need detailed explanations.

Mechanism 2: Vacancies in silicon are thought to be acceptors and their concentration is therefore expected to increase with phosphorus concentration, i.e., with the rise of the Fermi level towards the conduction band. Phosphorus-vacancy binding due to elastic and coulombic interactions is also expected. For these reasons, a considerable enhancement of the equilibrium vacancy concentration in highly *n*-type silicon is expected. During cooling while the new phase (i.e., P atoms) separates, the release of vacancies associated with P atoms should occur; this would create a supersaturation in vacancies which would be greater than that due to the change in temperature alone. The concentration of the negatively-charged vacancies in *n* type silicon is given by:

$$[C_{v-}]_n = [C_{v-}]_i \exp [(E_F - E_{F_i})/kT],$$
 where

 $[C_{v-}]_i$  = charged vacancy concentration in intrinsic silicon,

 $E_F$  = Fermi level in *n* type silicon, and

 $E_{F_i}$  = Fermi level in intrinsic silicon.

Table 3. Vacancy impurity interaction.

Solute	Ionic radius	$\Delta H_s, \ ev$	$_{ev}^{\Delta H_c,}$	$\Delta H = \Delta H_s + \Delta H_c,$ $ev$
P+ As+ B- Solvent Si	0.77 0.96 0.75 1.17	-0.165 -0.048 -0.247	-0.46 $-0.46$ $+0.46$	$     \begin{array}{r}       -0.63 \\       -0.51 \\       +0.21     \end{array} $

The value of  $[C_{v-}]_n/[C_{v-}]_i$  is estimated, using the Fermi level values given for various phosphorus concentrations and temperatures by Richter<sup>18</sup> to be  $\approx 130$  at 1000°C for silicon doped with  $10^{21}$  atoms/cm<sup>3</sup> of phosphorus. The elastic interaction energy  $\Delta H_S$  and the coulombic-interaction energy  $\Delta H_c$  for P<sup>+</sup>, B<sup>-</sup> and As<sup>+</sup> interacting with vacancies have been estimated by Swalin<sup>19</sup> and their values are shown in Table 3. The conclusion to be drawn from this table is that the vacancy concentrations due to impurity association effects will be higher when n-type impurities are involved. In the case of boron, however, there will be no increase in equilibrium concentration of vacancies due to "association" effects. A reasonable value of  $[C_{n-1}]_i$ will be  $\approx 10^{14}/\text{cm}^3$  at 1000°C. With phosphorus concentration in the surfaces reaching levels as high as 10<sup>21</sup> atoms/cm<sup>3</sup>,  $[C_{v-}]_n$  is expected to be  $\approx 10^{16}$ /cm<sup>3</sup>. Taking into account the impurity association effect (the vacancy increase due to this effect is  $\propto e^{-\Delta H/kT}$ ), a rough estimate for the total vacancy concentration  $C_v^0$  at  $1000^{\circ}$ C is expected to be  $10^{17}/\text{cm}^3$ . In the case of boron, this value is less than  $10^{14}/\text{cm}^3$ . Consequently the occurrence of helices due to vacancy supersaturations is expected in silicon diffused with large concentrations of phosphorus.

An estimate of the excess vacancy concentrations associated with formation of helices in our experiment can be made. The number of turns per unit length of a helix dislocation is related to the excess vacancy concentration by the formula<sup>20</sup>

$$n=rac{kT}{2\pi\mu b^4} \ln \, C_v/C_v^0,$$
 where

n = turns/length in cm,

 $C_v$  = actual vacancy concentration,

 $C_v^0$  = equilibrium vacancy concentration,

 $\mu = \text{modulus of rigidity, and}$ 

k = Boltzmann constant.

There exists a wide range of values of n in our observations due to the wedge shaped nature of diffused foils. The mean value of n estimated from Fig. 7 was found to be  $\approx 2 \times 10^5$ /cm. The corresponding value of  $C_v/C_v^0$  is  $\approx 10^2$ ,

which was obtained using the following values:  $\mu = 7.9 \times 10^{11} \text{ dynes/cm}^2$ , kT = 0.107 eV and  $b = 3.84 \times 10^{-8} \text{cm}$ . This would mean  $C_v$  at  $1000 \,^{\circ}\text{C}$  in local places in the matrix containing helices could reach as high as  $10^{19}/\text{cm}^3$  in phosphorus-diffused silicon.

Mechanism 3: If we assume that the second phase separates on cooling from a solid solution in which vacancies are not associated with solute atoms, and that the molar volume of the phase is less than the molar volume of the matrix, the particles of the phase will be surrounded by a stress field.<sup>20</sup> Vacancies in excess of the concentration which would be in thermal equilibrium at the temperature of precipitation might then be generated in the stressed region. The vacancies will be attracted in the compressed region of the crystal (i.e., within the precipitate) and consequently a flux of vacancies will be generated flowing towards the precipitates from the matrix.

Mechanism 4: During phosphorus diffusion at very high surface concentrations, the conversion of a part of the substitutional phosphorus atoms  $C_S$  into interstitials  $C_I$  and vacancies  $C_v$  according to the reaction

$$C_s \rightleftharpoons C_I + C_v \rightleftharpoons \sin ks$$

is expected to occur in silicon according to some researchers.<sup>21,22</sup> During phosphorus precipitation, if this mechanism is operative, a certain excess amount of vacancies is expected to be generated.

The operation of all these mechanisms in phosphorusdiffused silicon is likely. It is not possible to make a choice in favor of any one of these with the available evidence. It is certain, however, that the sources for creation of excess vacancies in heavily doped *n*-type silicon are far more efficiently operative than in silicon heavily doped with boron.

The role of vacancies in formation of zones is well known. A model by Federighi and Thomas<sup>23</sup> based upon vacancy-zone interaction is worth considering here. Because of some binding between a vacancy and an impurity atom, replacement of silicon atoms in a plane during the precipitation stage takes place by phosphorus atoms in association with vacancies. Some of the vacancies, however, will be released from the zones in order to collect more phosphorus atoms from the supersaturated matrix. This happens because the binding between vacancies and zones is neither zero nor infinite. The growth of zones is ultimately controlled by two processes—vacancies being evaporated from, and vacancies reaching, the zones. The former process is considered slow while the latter process is considered fast. The evidence for the existence of the latter process is provided by the observation of helices in phosphorus precipitate regions as seen in Fig. 6a at locations P, Q, R, etc. and the long helices extending from the precipitate region in Fig. 7. The phosphorus platelets observed in Fig. 6a are considered to be some of the zones that grew later into large or discrete precipitates which are coherent with the silicon matrix and probably belong to a metastable transition phase.

With phosphorus concentrations exceeding 10<sup>21</sup> atoms/cm<sup>3</sup>, very long and (sometimes) thick precipitate platelets (Figs. 4a-4c) were obtained. When the precipitates become thick, volume strain associated with them causes their tips to emit partial dislocations containing intrinsic stacking faults. The decoration of these faults with phosphorus clusters (Fig. 4d) is indicative of either strain relief during precipitation or of Suzuki-chemical interaction.

### • Boron precipitation

Boron precipitate platelets cause tension in the matrix similar to phosphorus. Dislocation helices running along  $\langle 220 \rangle$  directions (which are also the usual Burgers vector-directions) were, however, not observed. The helices of dislocation in the rod-type precipitate regions are thought not to be the helices originating from dislocations under large nonequilibrium vacancy concentrations. They are mismatch boundary envelopes, i.e., interface dislocations. This is indicated by the fact that the Burgers vector of these is not the usual  $(a/2) \langle 110 \rangle$  type.

The loss of coherency in precipitates of rod or three-dimensional shape in the silicon matrix is attended by the formation of dislocation envelopes. This is in accordance with the well known principle that the strain energy of a rod or cube-shape precipitate is much higher than that of a platelet-shape precipitate, assuming that the amount of precipitation and the accompanying volume change are held constant. The much smaller frequency of occurrence of rods and three-dimensional structures in comparison with that of the platelets is also consistent with this principle. The precipitate structures enveloped by dislocations and having no coherency with the silicon matrix are most probably composed of pure boron, since formation of  $\mathrm{Si}_z B_y$  phases at normal pressures is known to be improbable.

## **Conclusions**

Our investigations has shown that platelets of P and B precipitates are of the "vacancy" type, i.e., they cause tension in the matrix of silicon. Phosphorus and boron atoms are smaller in size than those of silicon, and, consequently, "vacancy" type precipitates are expected to form. These platelets cannot be said to belong to the equilibrium phases (such as SiP or  $Si_zB_y$ ) since these phases are known to possess higher specific volumes than that of silicon and are probably formed during the period of cooling from the diffusion temperature.

Phosphorus precipitates were found to be mostly platelets, whereas boron precipitates were observed to be rods, platelets, and three-dimensional. The frequency of the occurrence of the boron platelets was, however, much higher than that of rods and three-dimensional structures. Rods and three-dimensional structures were invariably found to be entwined by dislocation spirals considered to be interfacial dislocations.

Because the equilibrium vacancy concentration is much higher in silicon doped with phosphorus than in that doped with boron, the local nonequilibrium vacancy concentrations generated during P precipitation were of sufficient magnitude to cause dislocations to be converted into helices.

The origin of all the observed coherent discrete precipitate structures is thought to be the clustering phenomenon similar to that of Guinier-Preston zones. The observation of elongation of reciprocal points in the region of very thin precipitate structures of clusters gives credence to this thought.

#### **Acknowledgments**

The authors wish to thank Drs. T. H. Yeh and E. S. Wajda for valuable discussion and suggestions. We are grateful also to Mr. J. Lamot for his help in most of the experimental part of this work.

#### References

- 1. G. Thomas, Trans. AIME 233, 1608 (1965).
- P. F. Schmidt and R. Stickler, J. Electrochem. Soc. 111, 1188 (1964).
- M. L. Joshi, B. J. Masters and S. Dash, Appl. Phys. Letters 7, 306 (1965).
- 4. M. L. Joshi, J. Electrochem Soc. 113, 45 (1966).
- 5. J. C. Irvin, Bell System Tech. J. 41, 387 (1962).
- 6. B. Giessen and R. Vogel, Z. Metallkunde 5, 174, (1959).
- 7. W. Klemm and P. Pirshcer, Z. anorg. Chem. 211, 247 (1941).
- 8. F. A. Trumbore, Bell System Tech. J. 39, 205 (1960).
- J. Washburn, G. Thomas and H. J. Queisser, J. Appl. Phys. 35, 1909 (1964).
- 10. E. Tannenbaum, Sol. State Elect. 2, 123 (1961).
- P. B. Hirsch, A. Howie, R. B. Nicholson, D. W. Pashley and M. J. Whelan, *Electron Microscopy of Thin Crystals*, Butterworths, 1965, pp. 341-343.
- G. Thomas, Electron Microscopy of Thin Foils, University of California, Berkeley, California, Publication No. UCRL-11009, 1963, p. 14.
- 13. M. F. Ashby and L. M. Brown, *Phil. Mag.* 8, 1083 (1963).
- A. Howie and M. J. Whelan, Proc. Roy. Soc. A267, 206 (1962).
- 15. C. G. Beck and R. Stickler, to be published in J. Appl. Phys.
- A. S. Berezhonoi, Silicon and its Binary Systems, Consulants Bureau, New York, 1960 pp. 14–33.
- S. Amelinckx, The Direct Observations of Dislocations, Academic Press, New York, 1964, pp. 71–76, and 377–379.
- 18. Von E. Richter, Z. Naturforschg. 18a, 39 (1963).
- 19. R. A. Swalin, Journ. Appl. Phys. 29, 670 (1958).
- J. W. Mitchell, *Journ. Appl. Phys.* (Supplement to Vol.) 33, 406 (1962).
- 21. E. Kooi, Journ. Electrochem. Soc. 111, 1383 (1964).
- 22. S. Maekawa, Journ. Phys. Soc. Japan 17, 1592 (1962).
- 23. T. Federighi and G. Thomas, Phil. Mag. 7, 127 (1962).
- 24. H. Suzuki, Sci. Rep. Res. Inst. Tohoku Univ. A4, 455 (1952).
- A. S. Berezhonoi, Silicon and its Binary Systems, Consultants Bureau, New York, 1960 pp. 64–65.

Received November 11, 1966